Magnetic-optical core-shell nanostructures for highly selective photoelectrochemical aptasensing

Hongbo Li,[a,b] Yanli Li,[a] Jing Li,[a*] Fan Yang,[b] Lingqiu Xu,[a] Wei Wang,[a] Xiaxi Yao,[b] Yadong Yin[b*]

[a] *School of Chemistry and Chemical Engineering, Yancheng Institute of Technology, Yancheng 224051, PR China*

[b] *Department of Chemistry, University of California, Riverside, CA 92521, USA*

Tel: 951-827-4965; Fax: 951-827-4713

* E-mail: yadong.yin@ucr.edu (Y.Y.); jli@ycit.edu.cn (J.L).

Abstract: Selectivity is a crucial parameter for photoelectrochemical (PEC) sensing in a practical setting. Despite the use of specific probes such as aptamers, antibodies, and enzymes, coexisting interferences can still result in inaccuracies in PEC sensing, especially for complex biosample matrices. Here we report the design of a Fe_3O_4@SiO_2@TiO_2 magnetic-optical bifunctional beacon applied in a novel PEC sensor that can selectively capture progesterone in complex bio-samples, be magnetically separated and cleaned, and be detected in pure phosphate buffer solution (PBS). The magnetic separation strategy efficiently removes the complex coexisting species from the modified electrode surface and drastically enhances the selectivity of the as-designed PEC sensor. The as-designed PEC sensor is cost-effective, easy to fabricate, highly selective and sensitive, and highly reliable, making it a promising platform for efficient aptasensing.

***Keywords*:** Superparamagnetic, Core-shell, Photoelectrochemical, Aptasensing, Progesterone

Introduction

Photoelectrochemical (PEC) sensing, composed of separated light irradiation and electric signal readout, has attracted tremendous research interest in the past decade due to the high sensitivity resulting from its relatively low background signal response.[1] Development of PEC sensors has significantly focused on signal amplification strategies[2-3] to achieve higher sensitivity and lower limits of detection through the use of improved photoelectric beacons enhanced by metal ions doped semiconductors,[4] dyes or quantum dots sensitized semiconductors,[5-6] semiconductor heterojunctions,[7-12] and plasmonic nano-sized noble metals (Au, Ag) sensitized semiconductors.[13-16] Resonance energy transfer approaches have also been applied towards the construction of highly sensitive "on-off" type PEC sensors.[17-19] Furthermore, in order to develop ultrasensitive PEC aptasensing, various biological signal amplification strategies[20-23] were employed. All of these designs greatly contributed to the sensitivity of PEC sensing, resulting in a detection limit that can even reach the sub-femtomole level. To the best of our knowledge, however, there are few reports for PEC sensing with improved selectivity in real biological samples,[17, 24] especially for complex biosample matrices. As is known, the conventional detection approaches are typically based on analytes dropped on the surface of modified electrodes, incubated at 4 ^{o}C in a refrigerator overnight, then rinsed by a buffer to remove weakly binding target and coexisting species. Still, interferences are not easily removed due to the absorption and hydrogen bond interaction on the solid-liquid interfaces. While the electrode modified materials can be further removed following several washes, such an operation will result in problems in selectivity, reproducibility, and stability. We believe such shortcomings can be overcome by *in situ* magnetic separation and electrode assembly.

Superparamagnetic Fe_3O_4 nanocrystals have gained increasing interest due to their

paramagnetic response that can be fully controlled by externally applied magnetic fields,[25] holding promises for applications in recoverable enzyme-free catalysis,[26-28] magnetic resonance imaging,[29-30] cell separation,[31] drug delivery,[32] and therapy in biomedicine.[33] They can be well dispersed in solution after removing the external magnetic field,[34] and exhibit excellent biocompatibility and stability.[35-36] Due to their magnetic properties,[37] superparamagnetic Fe_3O_4 nanocrystals bound with specific probes can be applied for selectively extracting targets from a complex matrix by an external magnetic field, which is beneficial to improve the selectivity of PEC sensing.

In this work, we propose the design of a highly selective PEC aptasensing platform using bifunctional magnetic-optical core-shell superparamagnetic Fe_3O_4@SiO_2@TiO_2 nanoparticles modified with a progesterone aptamer and capture DNA (Scheme 1). When Fe_3O_4@SiO_2@TiO_2-NH_2-aptamer-cDNA nanoparticles capture the targets, the conformation of chain structured aptamer-cDNA will change,[38] blocking the incident light and decreasing the photocurrent. The superparamagnetic cores allow easy separation of the progesterone-captured nanoparticles and enable high selectivity for PEC sensing. With the advantages of high cost-effectiveness and ease of manufacture, as well as excellent performance in terms of selectivity, sensitivity, and repeatability, the as-fabricated PEC sensor has a broad prospect in monitoring progesterone in real biological environments.

Experimental section

Preparation of Fe_3O_4@SiO_2@TiO_2-NH_2-aptamer-cDNA

In the synthesis of Fe_3O_4@SiO_2@TiO_2-NH_2-aptamer-cDNA, 100 μL of 2 mol L^{-1} EDC and 5 mol L^{-1} NHS were added into 20 μL of aptamer Tris-HCl (50 mM, 150 mM NaCl, 2 mM $MgCl_2$, pH 7.4) solution for 1 h of the activation of carbonyl at room

temperature. Then 100 μL of Fe_3O_4@SiO_2@TiO_2-NH_2 suspension was added into the above solution at 4 °C overnight, and washed with Tris-HCl buffer solution several times by external magnetic force. Thus, Fe_3O_4@SiO_2@TiO_2-NH_2-aptamer was obtained and redispersed in 100 μL of Tris-HCl buffer solution. After that, 3.3 μL of 100 μmol L^{-1} cDNA Tris-HCl buffer solution was incubated with 100 μL of Fe_3O_4@SiO_2@TiO_2-NH_2-aptamer for 1 h of partial hybridization at 37 °C, and then the mixture was washed with Tris-HCl buffer solution several times by external magnetic force. Finally, Fe_3O_4@SiO_2@TiO_2-NH_2-aptamer-cDNA was produced and redispersed in 100 μL of Tris-HCl buffer solution. All the products modified with aptamer or cDNA were stored at 4 °C in refrigerator.

Determination of progesterone by prepared PEC sensor

Firstly, 100 μL solutions with different concentrations of progesterone were added into 100 μL of Fe_3O_4@SiO_2@TiO_2-NH_2-aptamer-cDNA Tris-HCl buffer solution. After the interaction of 40 min, the target was captured by Fe_3O_4@SiO_2@TiO_2-NH_2-aptamer-cDNA and removed from the solution by external magnetic force. Next, it was washed three times and redispersed in 100 μL of Tris-HCl buffer solution. After that, 20 μL of the above suspensions with different concentrations of progesterone were dropped on the cleaned ITO electrodes, respectively. When the modified electrodes were dried and they were used to draw a calibration curve. Finally, progesterone in liquid milk samples was also conducted by the same approach mentioned above, and then the concentration of progesterone was achieved by the calibration curve.

Results and discussion

Characterization and optimization

The morphologies and nanostructures of Fe_3O_4 nanoclusters, Fe_3O_4@SiO_2,

Fe_3O_4@SiO_2@TiO_2, and partially etched and calcined Fe_3O_4@SiO_2@TiO_2 have been imaged by HRTEM as displayed in Figure 1. The monodispersed Fe_3O_4 nanoclusters, with an average diameter of about 90 nm, are assembled from a large number of approximately 10 nm Fe_3O_4 nanocrystals (Figure 1A). In order to prevent the fragmentation of Fe_3O_4 nanoclusters and further titanium dioxide coating, Fe_3O_4 coated with SiO_2 was synthesized through the hydrolysis of TEOS, resulting in a silica shell with a thickness of about 40 nm which served as a moderate medium to tailor the lattice mismatch between Fe_3O_4 and TiO_2 (Figure 1B).[39] The Fe_3O_4@SiO_2@TiO_2 was then successfully prepared by hydrolysis of TBOT (Figure 1C), and the particle size increased to about 300 nm in diameter. To obtain a magnetic-optical composite with good photoelectric performance, the Fe_3O_4@SiO_2@TiO_2 was partially etched by NaOH solution, where the voids were then used for TiO_2 calcination shrinkage. The TiO_2 was calcined under nitrogen conditions, and the calcined Fe_3O_4@SiO_2@TiO_2 was about 240 nm in diameter (Figure 1D). To further confirm the successful synthesis of Fe_3O_4@SiO_2@TiO_2, the element mapping profiles have been displayed in Figure 2. The multicolor pattern of Figure 2A corresponded to Fe_3O_4@SiO_2@TiO_2. In addition, specific profiles of Fe (B), Si (C), Ti (D), and O (E) were reflected, respectively. For the element imaging profiles of Fe (B), Si (C), Ti (D), their dimensions increased accordingly, and their distributions were fully covered by the profile of O (E). These images all indicated that the Fe_3O_4@SiO_2@TiO_2 was successfully prepared.

X-ray diffraction (XRD) measurements were taken to confirm the structure of magnetic Fe_3O_4 nanoclusters, Fe_3O_4@SiO_2, and Fe_3O_4@SiO_2@TiO_2 (Figure 3A). As shown in curve a, the diffraction peaks located at 18.3°, 30.1°, 35.4°, 43.1°, 53.4°, 56.9°, 62.5°, and 74.9° can be assigned to the (111), (220), (311), (400), (422), (511), (440), and (622) planes of the magnetite Fe_3O_4 phase (JCPDS 19-0629).[35, 40] Curve b showed

the XRD pattern of annealed Fe_3O_4@SiO_2, and the positions of the peaks of Fe_3O_4 were almost the same as those of colloidal Fe_3O_4. However, those peaks' intensities were obviously enhanced, indicating that Fe_3O_4 saw improved crystallinity after being annealed at 600 ºC under nitrogen for 2 h. As seen in curve b, there was an additional broad peak at 16-30°, indicating that colloidal SiO_2 (JCPDS 29-0085) did not crystallize at 600 ºC. Compared to the curve b, additional peaks in curve c at 25.3°, 48.1°, and 55.1° can be assigned to the (101), (200), and (211) planes of anatase TiO_2 phase (JCPDS 21-1272).[41] The weak peak intensity is due to the thin-layer of TiO_2 coating the surface of Fe_3O_4@SiO_2. Therefore, the bifunctional magnetic-optical Fe_3O_4@SiO_2@TiO_2 was successfully prepared, ready to use for electrode modification and assembly.

The magnetic hysteresis loops measurements of Fe_3O_4, Fe_3O_4@SiO_2, and Fe_3O_4@SiO_2@TiO_2 were carried out at room temperature (Figure 3B). All the curves exhibited typical superparamagnetic characteristics as no obvious hysteresis, remanence, and coercivity appeared.[42] As can be seen from curve a, the saturation magnetization of Fe_3O_4 nanoclusters was 72 emu g^{-1}. When they were coated with a silica shell, the saturation magnetization decreased to 33 emu g^{-1} (curve b). The coating of massive diamagnetic silica diluted the magnetic response of Fe_3O_4 nanoclusters. When they were further coated with TiO_2 (curve c), the saturation magnetization further decreased to 20 emu g^{-1} due to the same principle. In order to discern the specific coercivities, the inset at the lower right corner of Figure 3B showed the amplified magnetic hysteresis loop. It exhibited that the small coercivities were all less than 15 Oe, indicating that the superparamagnetic properties at room temperature.[43]

The superparamagnetic features are essential for magnetic separation. As shown in the inset at the upper left corner of Figure 3B, the prepared magnetic

Fe_3O_4@SiO_2@TiO_2 microspheres can easily be dispersed in the solution and then readily removed from the substrate with an external magnetic field. Therefore, in view of this unique superparamagnetic feature, a probe was anchored to the Fe_3O_4@SiO_2@TiO_2 microspheres to allow for the magnetic separation of the analyte in complex biological samples.

Typically, the enhanced photocurrent is closely related to the amount of Fe_3O_4@SiO_2@TiO_2 modified ITO electrode. Therefore, the optimum amount of substance concentration has been investigated (Figure 4A). Firstly, Fe_3O_4@SiO_2@TiO_2 stock suspension was diluted multiple times. Then 20 μL of each diluted suspension was dropped onto the surface of ITO electrodes, dried under atmospheric conditions, and used for the photocurrent measurements. As seen from the curves a-d, the photocurrent gradually improved and reached the maximum until the stock solution was diluted 6 times. The photocurrent from curve e to curve g showed a downward trend, which corresponded to 7 ~ 9 times dilution. This expresses that a high concentration of Fe_3O_4@SiO_2@TiO_2 will result in the recombination of more photon-generated carriers and a low photocurrent. However, a low concentration of Fe_3O_4@SiO_2@TiO_2 does not produce adequate electrons separated from the holes. Therefore, the optimized dilution time of 6 was chosen for amino-group modification and DNA assembly.

In order to show that the Fe_3O_4@SiO_2@TiO_2 had been successfully modified with different species, impedance measurements were conducted at room temperature. As shown in Figure 5A, the surface of the Fe_3O_4@SiO_2@TiO_2 based glassy carbon electrodes was orderly modified with amidogen, aptamer, aptamer-cDNA, and then the combination of progesterone. The corresponding charge transfer resistance (R_{ct}) values were then read out from the semi-circle Nyquist plots (a-e). It can be seen that the diameter of a semi-circle Nyquist plot gradually increased with the Fe_3O_4@SiO_2@TiO_2

modified in sequence, indicating that the corresponding species were successfully assembled on its surface. Photocurrent measurements were also performed for the different modified ITO electrodes. As shown in Figure 5B, the photocurrent gradually decreased with the electrodes assembled by different species in sequence, which is caused by the blockage of the incident light to the surface of TiO_2 shells during the stepwise modification. Scheme 1 illustrates the proposed mechanism, in which the photocurrent decreases proportionally with the increase of progesterone concentration.

Analytical performance

The as-designed Fe_3O_4@SiO_2@TiO_2-NH_2-aptamer-cDNA combined with different concentrations of progesterone based photoanodes were used for the photocurrent measurements in 0.1 mol L^{-1} PBS (pH 7.0). As shown in Figure 6A, the photocurrents gradually decreased with the increase of progesterone concentration from 0 to 10000 pmol L^{-1}. A calibration curve was obtained through linear-fit (Figure 6B). The dynamic linear range was between 1 and 6000 pmol L^{-1}, and the limit of detection was 0.3 pmol L^{-1} at 3σ/k. Herein, σ is the standard deviation calibrated by blank photocurrent measurements for 7 times, and k is the slope of the calibration curve in Figure 6B. The low limit of detection is advantageous over all other detection methods reported in the literature (Table S1). This can be attributed to the intrinsic property of PEC sensing from having a low background signal. The linear range sees benefits of three orders of magnitude from the high-density assembly of Fe_3O_4@SiO_2@TiO_2-NH_2-aptamer-cDNA combined with progesterone on ITO electrodes. Additionally, the as-designed PEC sensor has good performance in cost-effectiveness, short time consumption, and simple operation.

For the as-designed PEC sensor, stability is one of the key parameters and has been tested (Figure 5B). Firstly, 100 μL of 100 pmol L^{-1} progesterone solution was added

into 100 μL of Fe_3O_4@SiO_2@TiO_2-NH_2-aptamer-cDNA Tris-HCl buffer solution. After 40 min, the target and Fe_3O_4@SiO_2@TiO_2-NH_2-aptamer-cDNA were separated by external magnetic force. It was then washed three times and redispersed in 100 μL of Tris-HCl buffer solution. 20 μL of the above suspension was dropped on the cleaned ITO electrodes and dried under atmospheric conditions in preparation for photocurrent measurements. There was almost no photocurrent change between the 3 times of switched illumination over 140 s, indicating that the fabricated PEC sensor had excellent stability. The shelf life of the as-designed PEC sensor was examined by keeping it in a refrigerator at 4 ˚C, and the photocurrent measurements were performed every week. The photocurrent was almost consistent with the initial value after 3 weeks, and was still maintained at a level of 94.3 % after storing for 4 weeks. This suggests that the fabricated PEC sensor can keep its stability for an even longer period of time. Another important parameter of reproducibility was also investigated. As can be seen in Figure 6B, a relative standard deviation of 5.2% was estimated from the calibration plots of seven freshly fabricated PEC sensors, indicating that the as-designed PEC sensors can be repeatedly produced.

Selectivity is a very important parameter for the PEC sensor. It was evaluated by conventional co-existing species such as norethisterone, 17β-estradiol, cortisol, estrone, quinolones, and estriol in liquid milk samples. As shown in Figure 4B, the maximum interference was no more than 6.8% even when we added norethisterone at 200 times the concentration of the target progesterone (10 pmol L^{-1}), 17β-estradiol (500 times), cortisol (500 times), estrone (500 times), quinolones (500 times), estriol (500 times), and a mixture of these species (each 100 times). The detailed experimental procedure was conducted using the same approach for progesterone determination with the involvement of co-existing species. The proportion of interference was calibrated by

the photocurrent induced by co-existing species. Good selectivity was attributed to the effective magnetic separation of the analyte in the presence of the interference substance and its detection in pure PBS.

Finally, the practicability of the Fe_3O_4@SiO_2@TiO_2-NH_2-aptamer-cDNA based PEC sensor was also estimated in real samples. Firstly, 100 μL of liquid milk was diluted with 500 μL of water, then 200 μL of Fe_3O_4@SiO_2@TiO_2-NH_2-aptamer-cDNA stock suspension was added and allowed to interact for 1h. It was then separated by an external magnetic field and washed several times. Afterward, it was redispersed in 200 μL of Tris-HCl buffer solution, and 20 μL of the above suspension was dropped onto clean ITO electrodes. After the modified electrode was dried under atmospheric conditions, it was used to take photocurrent measurements. A concentration of 201.4 pmol L^{-1} progesterone was obtained from the calibration curve (Table 1). A recovery between 97.5% and 103.7% was calculated with the standard addition method, indicating the high accuracy of the as-designed PEC sensor. The relative standard deviation of 1.86% suggests that the PEC sensor also has the advantage of high precision. Therefore, the as-designed PEC sensor can be successfully applied to detecting progesterone in a practical setting.

Conclusions

In this work, a novel and robust PEC sensor was developed based on magnetic-optical Fe_3O_4@SiO_2@TiO_2-NH_2-aptamer-cDNA nanoparticles. This strategy overcomes the issues of the conventional PEC process where complex coexisting species retain on the modified electrodes and obscure the detection. We believe the as-designed PEC sensor has a number of advantages, particularly in the easy separation of analytes from the complex biological sample by applying an external magnetic field which significantly enhances the selectivity since the PEC detection can be performed

in pure PBS. In addition, the superparamagnetic nature of the Fe_3O_4 cores offers the hybrid nanoparticles great dispersity in solution, which ensures high efficiency in capturing progesterone. The subsequent magnetic separation not only cleans the analytes but also allows their assembly in high density on the electrode, both of which are beneficial to high performance in PEC sensing of progesterone.

Acknowledgments

We acknowledge the financial support from the National Natural Science Foundation of China (21505117, 21775135, 21876144), the Natural Science Foundation of Jiangsu Province (BK20161309), and the Qinglan Project of Jiangsu Province. Yin is grateful for the financial support from the U.S. National Science Foundation (CHE-1808788).

Associated content

Supporting information

The detailed description regarding the reagents, apparatus, synthesis of Fe_3O_4, Fe_3O_4@SiO_2, Fe_3O_4@SiO_2@TiO_2, and Fe_3O_4@SiO_2@TiO_2-NH_2 particles can be found in the supporting information. This material is available free of charge via the Internet at http://pubs.acs.org.

Author information

Corresponding authors

* Tel: 951-827-4965; Fax: 951-827-4713; E-mail: yadong.yin@ucr.edu (Y.Y.)

* E-mail: jli@ycit.edu.cn (J.L.)

ORCID

Hongbo Li: 0000-0001-8662-0427

Yadong Yin: 0000-0003-0218-3042

Notes

The authors declare no competing financial interest.

References

1. Zhao, W. W.; Xu, J. J.; Chen, H. Y. Photoelectrochemical DNA biosensors. *Chem. Rev.* **2014,** *114*, 7421-7441.

2. Wang, J.; Xu, Q.; Xia, W. W.; Shu, Y.; Jin, D.; Zang, Y.; Hu, X. High sensitive visible light photoelectrochemical sensor based on in-situ prepared flexible Sn_3O_4 nanosheets and molecularly imprinted polymers. *Sensor. Actuat. B-Chem.* **2018**, *271*, 215-224.

3. Zhao, W. W.; Xu, J. J.; Chen, H. Y. Photoelectrochemical bioanalysis: the state of the art. *Chem. Soc. Rev.* **2015,** *44*, 729-741.

4. Yang, Q.; Hao, Q.; Lei, J.; Ju, H. Portable photoelectrochemical device integrated with self-powered electrochromic tablet for visual analysis. *Anal. Chem.* **2018,** *90*, 3703-3707.

5. Li, M.; Xiong, C.; Zheng, Y.; Liang, W.; Yuan, R.; Chai, Y. Ultrasensitive photoelectrochemical biosensor based on DNA tetrahedron as nanocarrier for efficient immobilization of CdTe QDs-methylene blue as signal probe with near-zero background noise. *Anal. Chem.* **2018,** *90*, 8211-8216.

6. Zeng, X.; Tu, W.; Li, J.; Bao, J.; Dai, Z. Photoelectrochemical biosensor using enzyme-catalyzed in situ propagation of CdS quantum dots on graphene oxide. *ACS Appl. Mater. Interfaces* **2014**, *6*, 16197-16203.

7. Zang, Y.; Hu, X.; Zhou, H.; Xu, Q.; Huan, P.; Xue, H. Enhanced photoelectrochemical behavior of CdS/WS_2 heterojunction for sensitive glutathione

biosensing in human serum. *Int. J. Electrochem. Sci.* **2018**, *13*, 7558-7570.

8. Hao, N.; Hua, R.; Zhang, K.; Lu, J.; Wang, K. A sunlight powered portable photoelectrochemical biosensor based on a potentiometric resolve ratiometric principle. *Anal. Chem.* **2018,** *90*, 13207-13211.

9. Li, P. P.; Cao, Y.; Mao, C. J.; Jin, B.; Zhu, J. J. A TiO_2/g-C_3N_4/CdS nanocomposite-based photoelectrochemical biosensor for ultrasensitive evaluation of T_4 polynucleotide kinase activity. *Anal. Chem.* **2018,** *91*, 3392-3399.

10. Li, H.; Li, J.; Xu, Q.; Hu, X. Poly(3-hexylthiophene)/TiO_2 nanoparticle-functionalized electrodes for visible light and low potential photoelectrochemical sensing of organophosphorus pesticide chlopyrifos. *Anal. Chem.* **2011,** *83*, 9681-9686.

11. Song, Z.; Fan, G. C.; Li, Z.; Gao, F.; Luo, X. Universal design of selectivity-enhanced photoelectrochemical enzyme sensor: integrating photoanode with biocathode. *Anal. Chem.* **2018,** *90*, 10681-10687.

12. Li, H.; Li, J.; Zhu, Y.; Xie, W.; Shao, R.; Yao, X.; Gao, A.; Yin, Y. Cd^{2+}-doped amorphous TiO_2 hollow spheres for robust and ultrasensitive photoelectrochemical sensing of hydrogen sulfide. *Anal. Chem.* **2018,** *90*, 5496-5502.

13. Shu, J.; Qiu, Z.; Lv, S.; Zhang, K.; Tang, D. Plasmonic enhancement coupling with defect-engineered TiO_{2-x}: a mode for sensitive photoelectrochemical biosensing. *Anal. Chem.* **2018,** *90*, 2425-2429.

14. Li, Z.; Su, C.; Wu, D.; Zhang, Z. Gold nanoparticles decorated hematite photoelectrode for sensitive and selective photoelectrochemical aptasensing of lysozyme. *Anal. Chem.* **2018,** *90*, 961-967.

15. Li, R.; Tu, W.; Wang, H.; Dai, Z. Near-infrared light excited and localized surface plasmon resonance-enhanced photoelectrochemical biosensing platform for cell analysis. *Anal. Chem.* **2018,** *90*, 9403-9409.

16. Ma, Z. Y.; Xu, F.; Qin, Y.; Zhao, W. W.; Xu, J. J.; Chen, H. Y. Invoking direct exciton-plasmon interactions by catalytic Ag deposition on Au nanoparticles: photoelectrochemical bioanalysis with high efficiency. *Anal. Chem.* **2016,** *88*, 4183-4187.

17. Zhang, N.; Shi, X. M.; Guo, H. Q.; Zhao, X. Z.; Zhao, W. W.; Xu, J. J.; Chen, H. Y. Gold nanoparticle couples with entropy-driven toehold-mediated DNA strand displacement reaction on magnetic beads: toward ultrasensitive energy-transfer-based photoelectrochemical detection of miRNA-141 in real blood sample. *Anal. Chem.* **2018,** *90*, 11892-11898.

18. Wang, Z.; Liu, J.; Liu, X.; Shi, X.; Dai, Z. Photoelectrochemical approach to apoptosis evaluation via multi-functional peptide- and electrostatic attraction-guided excitonic response. *Anal. Chem.* **2019,** *91*, 830-835.

19. Zayats, M.; Kharitonov, A. B.; Pogorelova, S. P.; Lioubashevski, O.; Katz, E.; Willner, I. Probing photoelectrochemical processes in Au-CdS nanoparticle arrays by surface plasmon resonance: application for the detection of acetylcholine esterase inhibitors. *J. Am. Chem. Soc.* **2003,** *125*, 16006-16014.

20. Hou, T.; Xu, N.; Wang, W.; Ge, L.; Li, F. Truly immobilization-free diffusivity-mediated photoelectrochemical biosensing strategy for facile and highly sensitive microRNA assay. *Anal. Chem.* **2018,** *90*, 9591-9597.

21. Zheng, Y. N.; Liang, W. B.; Xiong, C. Y.; Zhuo, Y.; Chai, Y. Q.; Yuan, R. Universal ratiometric photoelectrochemical bioassay with target-nucleotide transduction-amplification and electron-transfer tunneling distance regulation strategies for ultrasensitive determination of microRNA in cells. *Anal. Chem.* **2017,** *89*, 9445-9451.

22. Ye, C.; Wang, M. Q.; Luo, H. Q.; Li, N. B. Label-free photoelectrochemical "off-on" platform coupled with g-wire-enhanced strategy for highly sensitive microRNA

sensing in cancer cells. *Anal. Chem.* **2017,** *89*, 11697-11702.

23. Li, C. X.; Lu, W. S.; Zhu, M.; Tang, B. Development of visible-light induced photoelectrochemical platform based on cyclometalated iridium(111) complex for bioanalysis. *Anal. Chem.* **2017,** *89*, 11098-11106.

24. Zhang, X.; Zhao, Y.; Li, S.; Zhang, S. Photoelectrochemical biosensor for detection of adenosine triphosphate in the extracts of cancer cells. *Chem. Commun.* **2010,** *46*, 9173-9175.

25. Wu, L.; Mendoza-Garcia, A.; Li, Q.; Sun, S. Organic phase syntheses of magnetic nanoparticles and their applications. *Chem. Rev.* **2016,** *116*, 10473-10512.

26. Jiang, B.; Duan, D.; Gao, L.; Zhou, M.; Fan, K.; Tang, Y.; Xi, J.; Bi, Y.; Tong, Z.; Gao, G. F.; Xie, N.; Tang, A.; Nie, G.; Liang, M.; Yan, X. Standardized assays for determining the catalytic activity and kinetics of peroxidase-like nanozymes. *Nat. Protoc.* **2018,** *13*, 1506-1520.

27. Huo, M.; Wang, L.; Chen, Y.; Shi, J. Tumor-selective catalytic nanomedicine by nanocatalyst delivery. *Nat. Commun.* **2017,** *8*, 357, 1-12.

28. Liang, M.; Fan, K.; Pan, Y.; Jiang, H.; Wang, F.; Yang, D.; Lu, D.; Feng, J.; Zhao, J.; Yang, L.; Yan, X. Fe_3O_4 Magnetic nanoparticle peroxidase mimetic-based colorimetric assay for the rapid detection of organophosphorus pesticide and nerve agent. *Anal. Chem.* **2013,** *85*, 308-312.

29. Zhao, H. X.; Zou, Q.; Sun, S. K.; Yu, C.; Zhang, X.; Li, R. J.; Fu, Y. Y. Theranostic metal-organic framework core-shell composites for magnetic resonance imaging and drug delivery. *Chem. Sci.* **2016,** *7*, 5294-5301.

30. Tian, Q.; Hu, J.; Zhu, Y.; Zou, R.; Chen, Z.; Yang, S.; Li, R.; Su, Q.; Han, Y.; Liu, X. Sub-10 nm Fe_3O_4@$Cu_{2-x}S$ core-shell nanoparticles for dual-modal imaging and photothermal therapy. *J. Am. Chem. Soc.* **2013,** *135*, 8571-8577.

31. Dutta Chowdhury, A.; Agnihotri, N.; Doong, R. a.; De, A., Label-free and nondestructive separation technique for isolation of targeted DNA from DNA-protein mixture using magnetic Au-Fe_3O_4 nanoprobes. *Anal. Chem.* **2017,** *89*, 12244-12251.

32. Li, W. P.; Liao, P. Y.; Su, C. H.; Yeh, C. S. Formation of oligonucleotide-gated silica shell-coated Fe_3O_4-Au core-shell nanotrisoctahedra for magnetically targeted and near-infrared light-responsive theranostic platform. *J. Am. Chem. Soc.* **2014,** *136*, 10062-10075.

33. Yin, T.; Wu, H.; Zhang, Q.; Gao, G.; Shapter, J. G.; Shen, Y.; He, Q.; Huang, P.; Qi, W.; Zhang, C.; Yang, Y.; Cui, D. In vivo targeted therapy of gastric tumors via the mechanical rotation of a flower-like Fe_3O_4@Au nanoprobe under an alternating magnetic field. *Npg Asia Mater.* **2017,** *9*, e408, 1-10.

34. Ge, J.; Hu, Y.; Yin, Y. Highly tunable superparamagnetic colloidal photonic crystals. *Angew. Chem. Int. Edit.* **2007,** *46*, 7428-7431.

35. Ge, J.; Hu, Y.; Biasini, M.; Beyermann, W. P.; Yin, Y. Superparamagnetic magnetite colloidal nanocrystal clusters. *Angew. Chem. Int. Edit.* **2007,** *46*, 4342-4345.

36. Zhao, L.; Qin, H.; Hu, Z.; Zhang, Y.; Wu, R. a.; Zou, H. A poly(ethylene glycol)-brush decorated magnetic polymer for highly specific enrichment of phosphopeptides. *Chem. Sci.* **2012,** *3*, 2828-2838.

37. Ranc, V.; Markova, Z.; Hajduch, M.; Prucek, R.; Kvitek, L.; Kaslik, J.; Safarova, K.; Zboril, R. Magnetically assisted surface-enhanced raman scattering selective determination of dopamine in an artificial cerebrospinal fluid and a mouse striatum using Fe_3O_4/Ag nanocomposite. *Anal. Chem.* **2014,** *86*, 2939-2946.

38. Jimenez, G. C.; Eissa, S.; Ng, A.; Alhadrami, H.; Zourob, M.; Siaj, M. Aptamer-based label-free impedimetric biosensor for detection of progesterone. *Anal. Chem.* **2015,** *87*, 1075-1082.

39. Yang, D.; Pang, X.; He, Y.; Wang, Y.; Chen, G.; Wang, W.; Lin, Z. Precisely size-tunable magnetic/plasmonic core/shell nanoparticles with controlled optical properties. *Angew. Chem. Int. Edit.* **2015,** *54*, 12091-12096.

40. Peng, S.; Sun, S. Synthesis and characterization of monodisperse hollow Fe_3O_4 nanoparticles. *Angew. Chem. Int. Edit.* **2007,** *46*, 4155-4158.

41. Schneider, J.; Matsuoka, M.; Takeuchi, M.; Zhang, J.; Horiuchi, Y.; Anpo, M.; Bahnemann, D. W. Understanding TiO_2 photocatalysis: mechanisms and materials. *Chem. Rev.* **2014,** *114*, 9919-9986.

42. Zhao, X.; Cai, Y.; Wang, T.; Shi, Y.; Jiang, G. Preparation of alkanethiolate-functionalized core/shell Fe_3O_4@Au nanoparticles and its interaction with several typical target molecules. *Anal. Chem.* **2008,** *80*, 9091-9096.

43. Peng, S.; Lei, C.; Ren, Y.; Cook, R. E.; Sun, Y. Plasmonic/magnetic bifunctional nanoparticles. *Angew. Chem. Int. Edit.* **2011,** *50*, 3158-3163.

Figure and table captions

Scheme 1. Schematic illustration of the synthesis of Fe_3O_4@SiO_2@TiO_2 modified with aptamer and capture DNA for PEC aptasensing of progesterone.

Figure 1. HRTEM images of Fe_3O_4 (A), Fe_3O_4@SiO_2 (B), Fe_3O_4@SiO_2@TiO_2 (C) without annealing, and Fe_3O_4@SiO_2@TiO_2 microspheres calcined at 600 ˚C for 2 h in N_2 atmosphere (D).

Figure 2. Elemental mappings of Fe_3O_4@SiO_2@TiO_2 core-shell-shell structures (A), Fe (B), Si (C), Ti (D), O (E) corresponding to the image of (A).

Figure 3. (A) X-ray diffraction patterns of (a) magnetite Fe_3O_4 particles without calcination, (b) Fe_3O_4@SiO_2, and (c) Fe_3O_4@SiO_2@TiO_2 particles calcined at 600 °C for 2 h in N_2 atmosphere. (B) Magnetic hysteresis loops of (a) Fe_3O_4, (b) Fe_3O_4@SiO_2,

and (c) Fe_3O_4@SiO_2@TiO_2 particles measured at room temperature. The inset at the upper left corner is a photo showing the superparamagnetic behavior of the Fe_3O_4@SiO_2@TiO_2 particles in response to an external magnetic field. The inset at the lower right corner shows an enlarged portion of the magnetic hysteresis curves.

Figure 4. (A) Curve a to g corresponds to the photocurrent response of the crystalline Fe_3O_4@SiO_2@TiO_2 microspheres that have been diluted 3 to 9 times. (B) The interference of 200-fold norethisterone, 500-fold 17β-estradiol, 500-fold cortisol, 500-fold estrone, 500-fold quinolones, 500-fold estriol, and 100-fold concentration of each of these species for Fe_3O_4@SiO_2@TiO_2-NH_2-aptamer-cDNA modified ITO electrodes at a bias potential of 0.1 V and in 0.1 mol L^{-1} PBS (pH 7.0).

Figure 5. (A) Electrochemical impedance spectra measured in 2.5 mmol L^{-1} $[Fe(CN)_6]^{4-/3-}$ solution containing 0.2 mol L^{-1} KNO_3 based on the glassy carbon electrodes modified with Fe_3O_4@SiO_2@TiO_2 (a), Fe_3O_4@SiO_2@TiO_2-NH_2 (b), Fe_3O_4@SiO_2@TiO_2-NH_2-aptamer (c), Fe_3O_4@SiO_2@TiO_2-NH_2-aptamer-cDNA (d), and Fe_3O_4@SiO_2@TiO_2-NH_2-aptamer-cDNA combined with 100 pmol L^{-1} progesterone (e). (B) The modified photoanode corresponds to the photocurrent response in 0.1 mol L^{-1} PBS (pH 7.0) and at a bias potential of 0.1 V.

Figure 6. (A) The photocurrent responses of Fe_3O_4@SiO_2@TiO_2-NH_2-aptamer-cDNA combined with 0, 1, 2, 4, 6, 8, 10, 20, 40, 60, 80, 100, 200, 400, 600, 800, 1000, 2000, 4000, 6000, 8000 and 10000 pmol L^{-1} progesterone in 0.1 mol L^{-1} PBS (pH 7.0) and at a bias potential of 0.1 V. (B) The linear calibration curve.

Table 1. Analytical results of progesterone in liquid milk samples using the proposed method (n=4).

Scheme 1

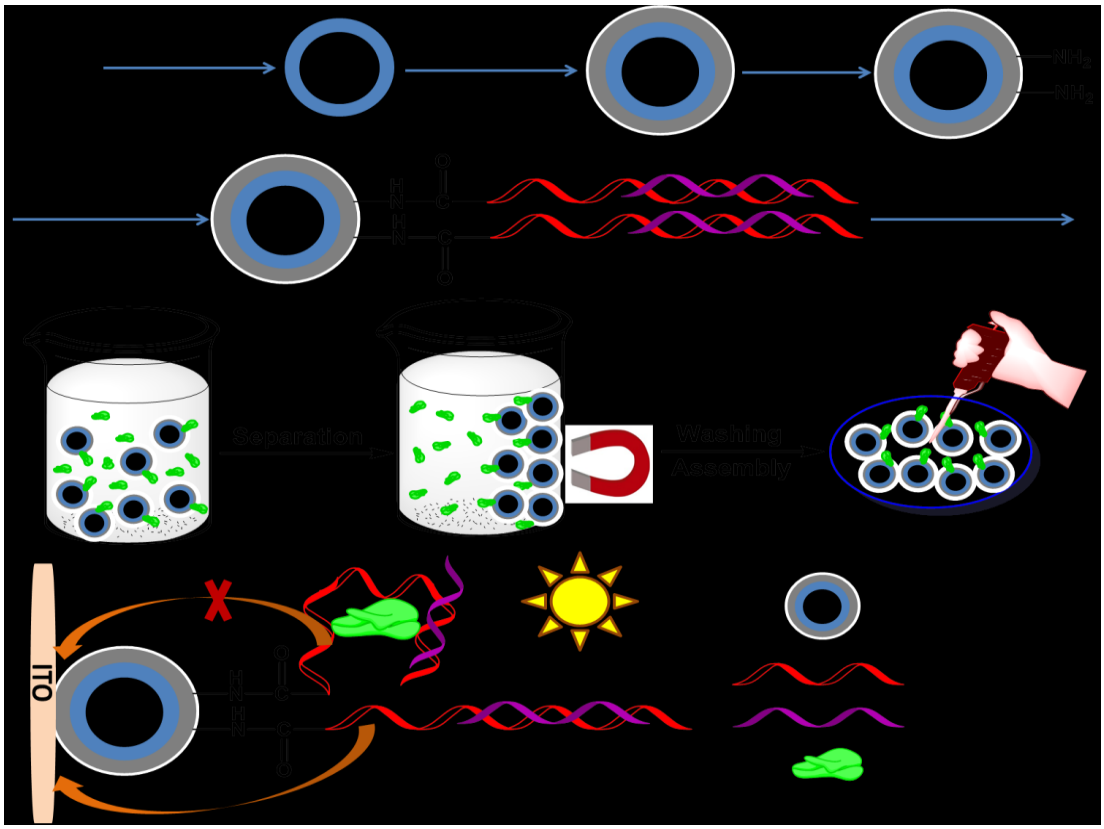

Figure 1

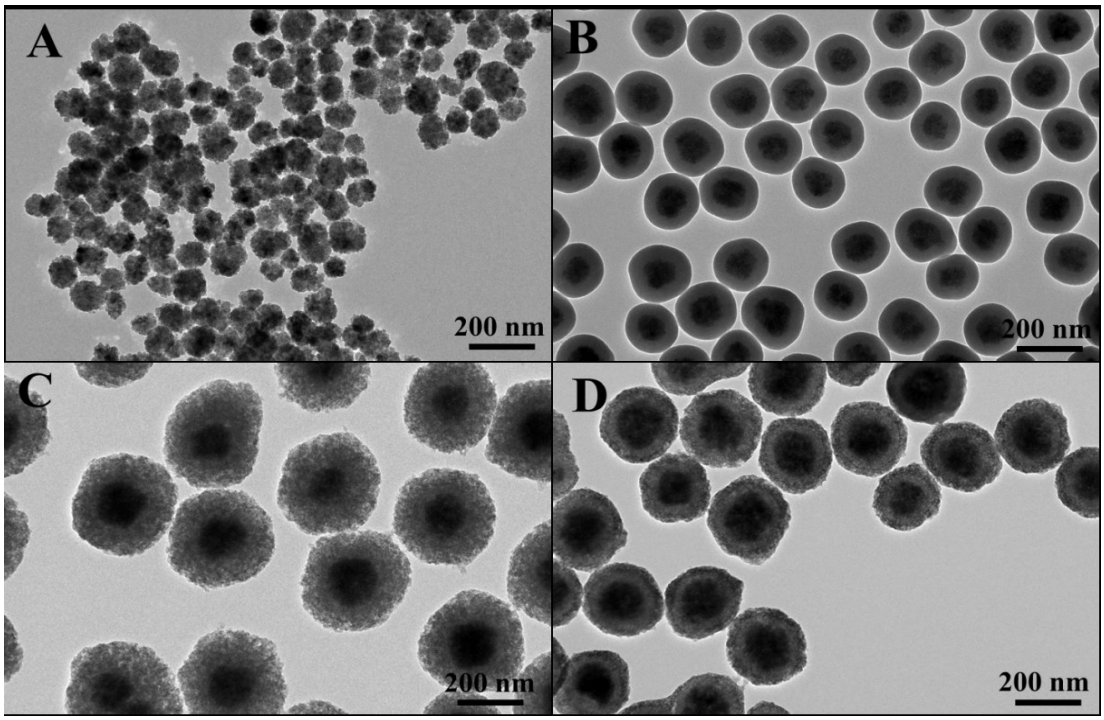

Figure 2

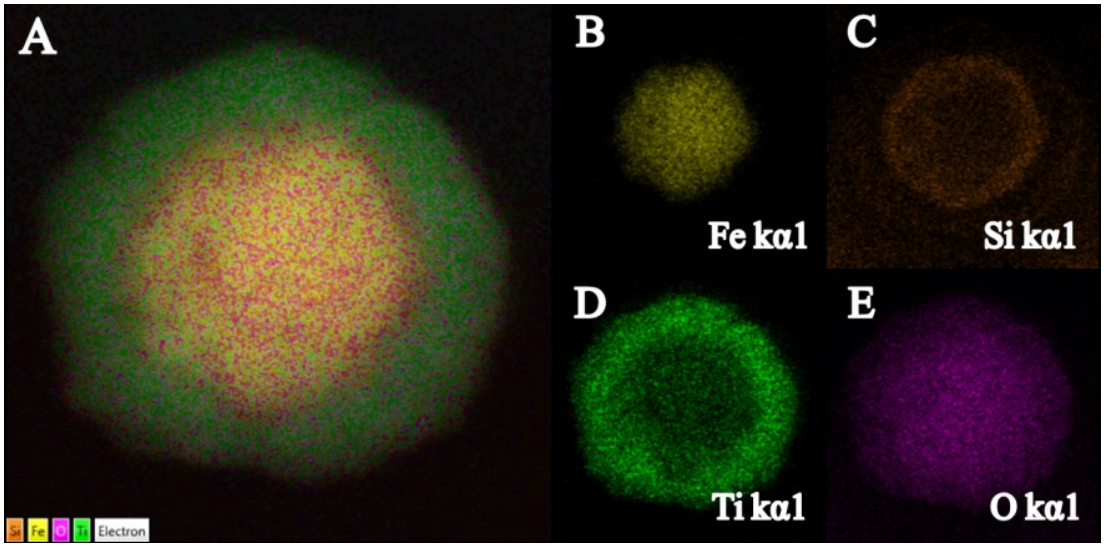

Figure 3

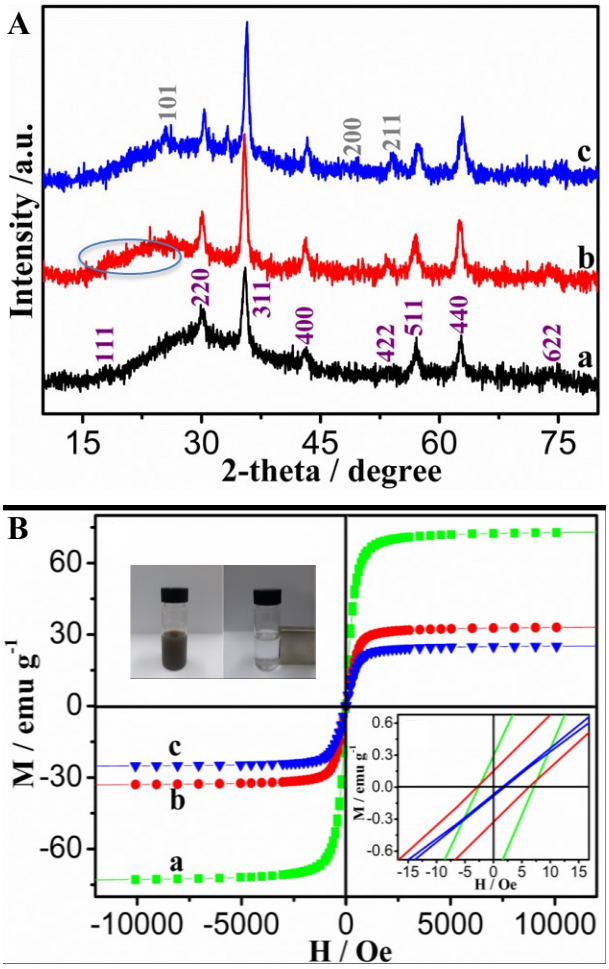
A
Intensity /a.u.
101
200
211
c
b
220
311
400
422
511
440
622
111
a
15
30
45
60
75
2-theta / degree
B
60
30
0
-30
-60
M / emu g-1
c
b
a
-10000
-5000
0
5000
10000
H / Oe
0.6
0.3
0.0
-0.3
-0.6
M / emu g-1
-15
-10
-5
0
5
10
15
H / Oe

Figure 4

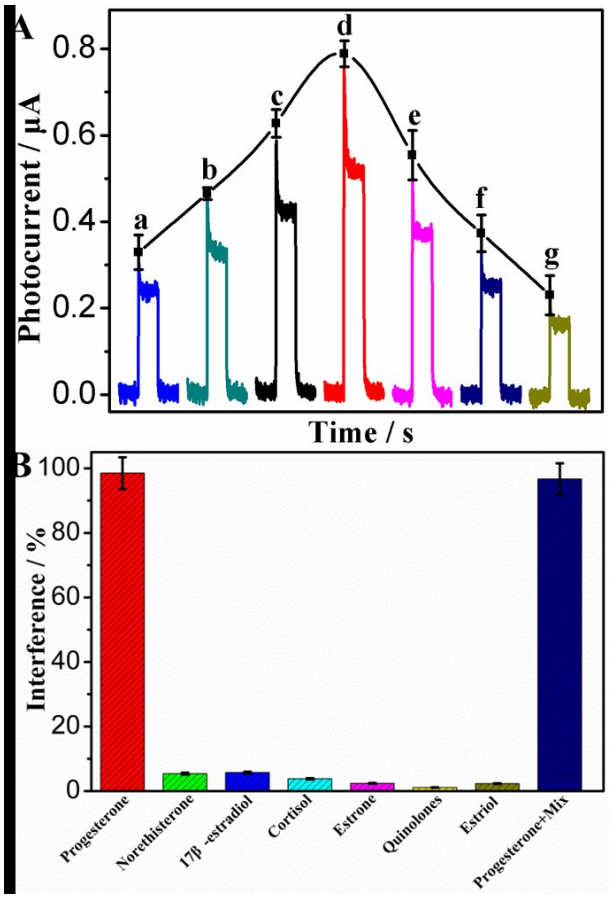
A
Photocurrent / μA
0.0
0.2
0.4
0.6
0.8
a
b
c
d
e
f
g
Time / s
B
Interference / %
0
20
40
60
80
100
Progesterone
Norethisterone
17β -estradiol
Cortisol
Estrone
Quinolones
Estriol
Progesterone+Mix

Figure 5

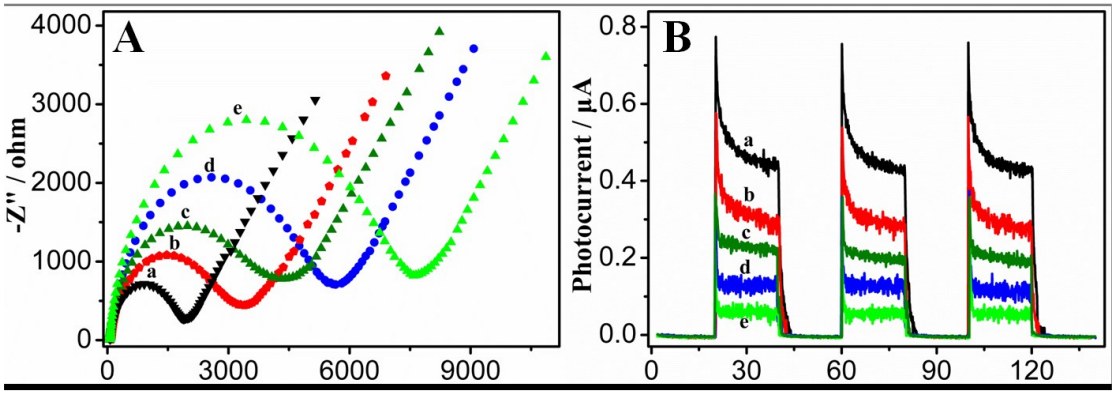
A
-Z'' / ohm
4000
3000
2000
1000
0
0
3000
6000
9000
a
b
c
d
e
B
Photocurrent / μA
0.8
0.6
0.4
0.2
0.0
0
30
60
90
120
a
b
c
d
e

Figure 6

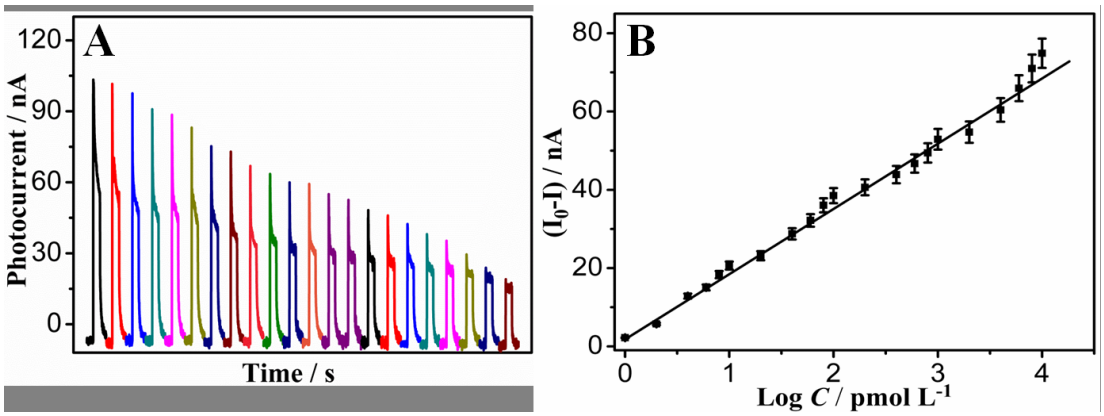
A
Photocurrent / nA
120
90
60
30
0
Time / s
B
(I_0-I) / nA
80
60
40
20
0
0
1
2
3
4
Log C / pmol L^{-1}

Table 1

Sample	Added (pmol L^{-1})	Found (pmol L^{-1})	Recovery (%)	RSD (%)
Liquid milk	0	201.4	---	0.68
	200	408.7	103.7	1.86
	400	599.5	99.5	1.54
	600	787	97.6	1.34
	800	981	97.5	1.50

n is the number of repetitive measurements.

TOC